

Andreas Biffar  
Andrea Baur-Melnyk  
Gerwin P. Schmidt  
Maximilian F. Reiser  
Olaf Dietrich

## Multiparameter MRI assessment of normal-appearing and diseased vertebral bone marrow

Received: 9 February 2010  
Revised: 12 April 2010  
Accepted: 23 April 2010  
Published online: 17 June 2010  
© European Society of Radiology 2010

A. Biffar · M. F. Reiser · O. Dietrich (✉)  
Josef Lissner Laboratory for Biomedical  
Imaging, Institute of Clinical Radiology,  
LMU University Hospitals Munich-  
Grosshadern,  
Marchioninstr. 15, 81377 Munich,  
Germany  
e-mail: od@dtrx.net  
Tel.: +49-89-70954622  
Fax: +49-89-70954627

A. Baur-Melnyk · G. P. Schmidt ·  
M. F. Reiser  
Institute of Clinical Radiology,  
LMU University Hospitals Munich-  
Grosshadern,  
Marchioninstr. 15, Munich 81377, Germany

**Abstract** *Objective:* To evaluate spin-lattice (T1) and spin-spin (T2) relaxation times as well as apparent diffusion coefficients (ADCs) of the fat and water components in the vertebral bone marrow (vBM) of patients with benign and malignant lesions. *Methods:* Forty-four patients were examined at 1.5 T: there were 24 osteoporotic vertebral fractures (15 women, 9 men; median age: 73, 48–86 years) and 20 malignant vertebral infiltrations (9 women, 11 men; median age: 60, 25–87). Relaxation times were determined separately for the water and the fat component using a saturation-recovery technique for T1 and measurements with variable echo times for T2. ADCs were determined with a diffusion-weighted (DW) echo-planar imaging (EPI) and a single-shot turbo-spin-echo (ssTSE) sequence. *Results:* T1 of the water component and ADCs were significantly increased in the lesions

compared with normal-appearing vBM (malignant: 1,252 vs. 828 ms, osteoporotic: 1,315 vs. 872 ms). ADCs determined with the DW-ssTSE were significantly increased compared with the DW-EPI. ADCs determined with the DW-ssTSE differed significantly between osteoporotic and malignant lesions ( $1.74$  vs  $1.35 \times 10^{-3}$  mm<sup>2</sup>/s).

*Conclusions:* All parameters exhibit significant differences between normal-appearing vBM and the lesions. However, only the ADCs determined with the DW-ssTSE differed significantly between osteoporotic fractures and malignant lesions, potentially allowing for a differential diagnosis of these two entities.

**Keywords** Magnetic resonance imaging · Relaxation times · Diffusion · Vertebral bone marrow · Vertebral fractures

### Introduction

Magnetic resonance imaging (MRI) plays an integral role in the detection and characterisation of bone marrow lesions. The evaluation of pathological features of vertebral bone marrow (vBM) with MRI is performed using standard T1- or T2-weighted and short-tau inversion-recovery (STIR) sequences.

The signal characteristics of vBM are mainly dominated by the distribution pattern of its constituents, namely yellow and red marrow [1]. Yellow marrow mainly consists of fat, while red marrow consists of comparable amounts of fat and water. Image contrast in MRI depends

on the relaxation characteristics and in diffusion-weighted (DW) sequences also on the diffusion coefficients of the underlying tissue. These characteristics are known to be different for protons in water and fat. Fat exhibits a very efficient spin-lattice relaxation resulting in a short T1 relaxation time [2] and a relatively long T2 relaxation time [3]. T1 of the water component is relatively long compared to the fat component, while T2 is shorter [4]. The diffusivity, measured in terms of the apparent diffusion coefficient (ADC), of fat protons is almost negligible, while it is very high in water. Bulk T1 and T2 relaxation times [5–7] and ADCs [8–12] of vBM were determined in various studies, reflecting average param-

ters of both components without permitting them to be separated. Only a few studies separately determined the parameters for the fat and water components in normal vBM as well as in pathological conditions [13–15].

Benign (osteoporosis) or malignant (tumor or metastasis) causes of acute vertebral collapse are often difficult to differentiate. An accurate diagnosis is important for appropriate treatment and prognosis. Studies based on signal intensities in STIR or non-contrast-enhanced and contrast-enhanced T1-weighted images as well as on morphological characteristics of the lesions [16–22] have been performed, yielding promising results with accuracies up to 95%. However, these results are based on qualitative criteria, depending on the sequence setup and the experience of the reader. Since both pathologies are expected to change the tissue physiology differently, quantitative imaging might therefore be able to differentiate between benign and malignant lesions and overcome the limitations of qualitative

criteria. T2 [14, 23, 24], T1 [14, 23] and especially the ADC [25–31] were evaluated in this context.

The purpose of this study was the separate measurement of ADC, T1 and T2 of the fat and water components. Measurements were performed in patients with normal-appearing vBM as well as with benign and malignant vertebral lesions in order to analyse the effects of various pathological processes on the physical properties of the bone-marrow components.

## Materials and methods

### Patients

After internal review board approval and informed consent had been received, 44 patients were examined.

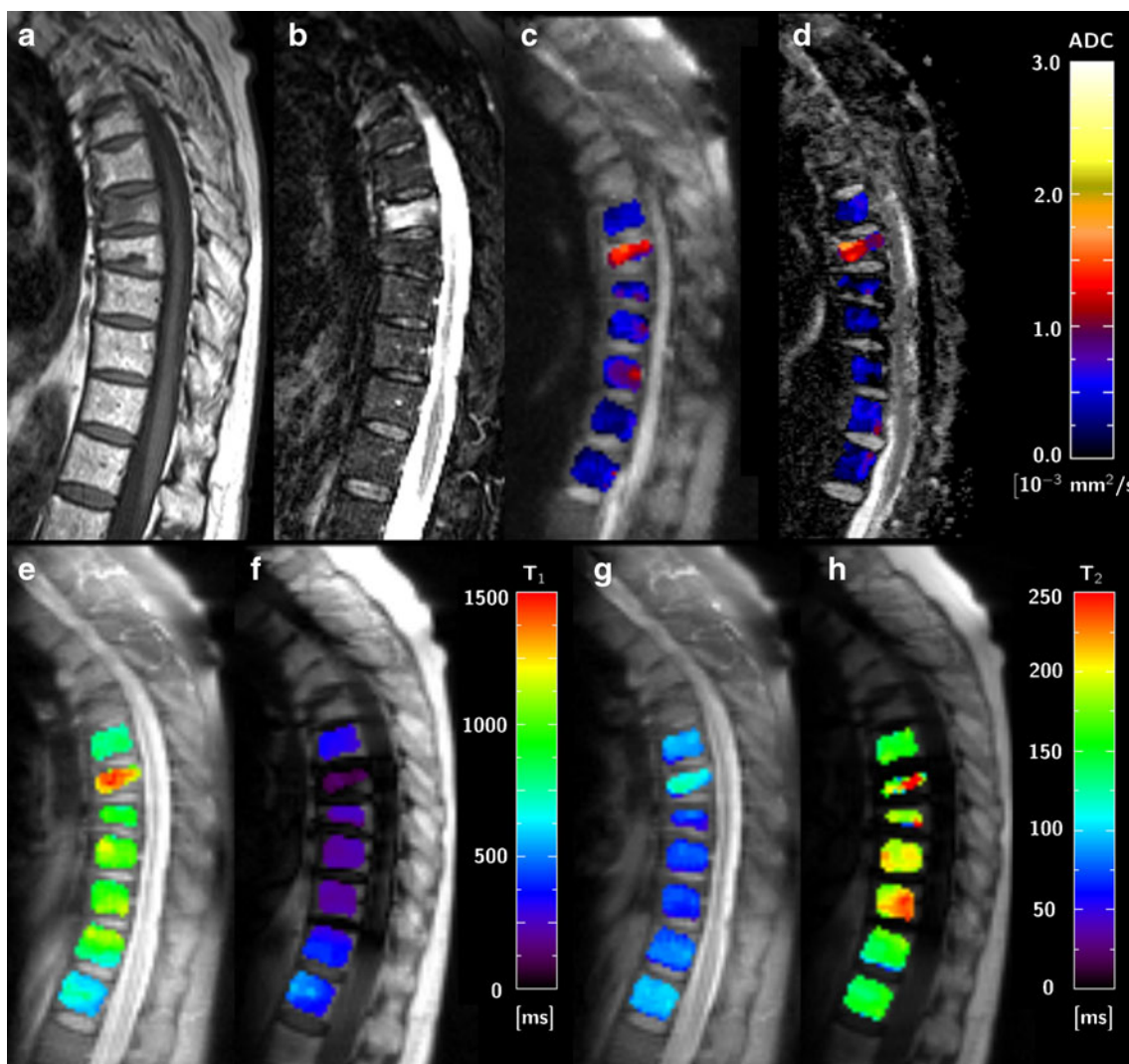


**Fig. 1** (a) T1-weighted TSE and (b) STIR images of a patient with an osteoporotic fracture in T7 and the corresponding parameter maps of the ADC determined with (c) the DW-ssTSE and (d) the

DW-EPI sequence as well as the (e) T1 water, (f) T1 fat, (g) T2 water and (h) T2 fat are shown

Patients were divided into groups according to the cause of the acute vertebral fracture. Group 1 consisted of 24 benign fractures in 24 patients with osteoporosis (15 women and 9 men, median age: 73 years, range: 48–86 years). The presence of a tumour in these patients was ruled out by follow-up MR examinations or multidetector computed-tomography (CT) examinations. Group 2 consisted of 20 malignant infiltrations in 20 patients (9 women and 11 men, median age: 60 years, range: 25–87 years) accompanied by pathological fractures in 12 of these 20 cases. Primary neoplasms included multiple myeloma ( $n=7$ ), breast cancer ( $n=5$ ), adenocarcinoma ( $n=3$ ), ovarian cancer ( $n=1$ ), hypopharyngeal cancer ( $n=1$ ), thyroid carcinoma ( $n=1$ ), bladder cancer ( $n=1$ ) and non-seminoma ( $n=1$ ). The diagnoses were confirmed with histopathological examination of specimens obtained during surgery, CT-guided biopsy or follow-up MR examinations. Patients without an acute bone-marrow oedema in fracture sites were excluded.

#### Magnetic resonance imaging

Measurements were performed on a 1.5-T whole-body system (MAGNETOM Avanto, Siemens Healthcare, Erlangen, Germany) using a quadrature spine surface coil. T1-weighted (TR/TE, 531/12 ms), STIR (TR/TE/TI, 3790/61/180 ms) and T2-weighted (TR/TE, 4420/118 ms) turbo-spin-echo images of 21 sagittal slices with a slice thickness of 3.0 mm were acquired using a  $44 \times 44 \text{ cm}^2$  field of view (FOV) and a matrix size of  $384 \times 384$ , and used for lesion localisation and proper slice positioning in the following measurements.

A sagittal slice centred on the lesion with a slice thickness of 5.0 mm and a FOV of  $30 \times 22 \text{ cm}^2$  was selected. First, ADCs were determined with a fat-saturated diffusion-weighted single-shot turbo-spin-echo (DW-ssTSE) sequence (TR/TE, 3,000/72 ms) with four different  $b$ -values ( $b=100, 250, 400, 600 \text{ s/mm}^2$ ) and matrix size:  $128 \times 92$ , flip angle:  $180^\circ$  for the refocusing pulses, and a bandwidth of 735 Hz/pixel. Diffusion

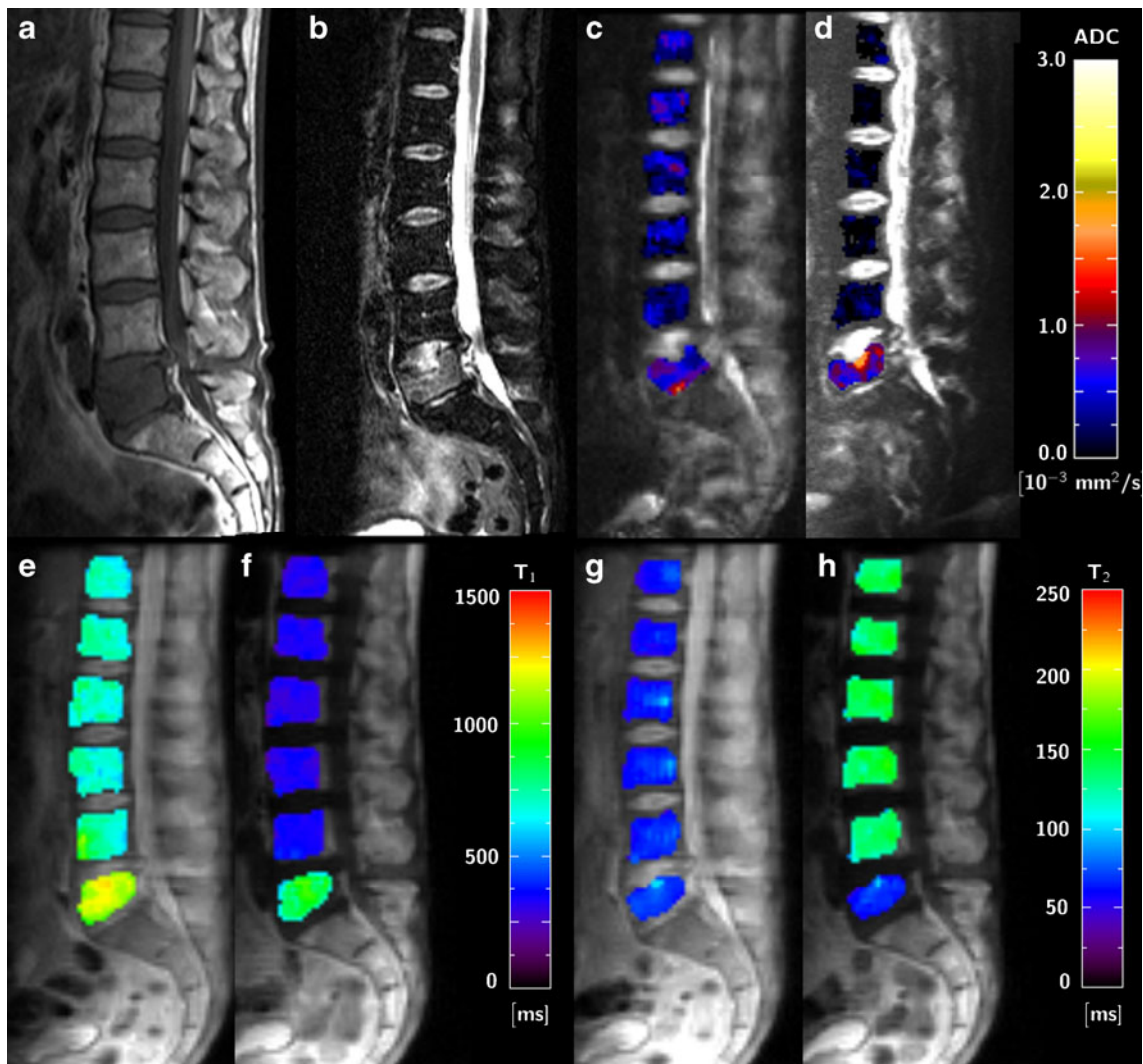


**Fig. 2** The same images as in Fig. 1 but for a patient with a malignant lesion in L5

gradients were applied in all three physical gradient directions simultaneously to achieve a maximum gradient amplitude and diffusion weighting. Because of the low signal of the bone marrow in DWI, ten averages were taken in order to improve the signal-to-noise ratio (SNR). Second, a fat-saturated diffusion-weighted echo-planar imaging (DW-EPI) sequence (TR/TE, 3,000/87 ms,  $b=50, 300, 600$  s/mm<sup>2</sup>) was performed with a matrix size of 192×144 and a bandwidth of 965 Hz/pixel. The diffusion signals were averaged over five repeated acquisitions and three orthogonal gradient directions. In both measurements, the b-value was varied by a change of the diffusion-gradient amplitude keeping the gradient duration constant.

T1 of the water and fat component were determined with a saturation-recovery (SR) half-Fourier-acquisition single-shot turbo-spin-echo (HASTE) sequence (saturation times TI=5, 50, 100, 200, 400, 800, 1,600 and 3,200 ms) preceded by either a fat- or water-saturation pulse,

respectively. T2 was measured using a HASTE sequence with varying echo times (TE=14, 28, 69, 99, 130 and 170 ms) preceded by either a fat- or water-saturation pulse, respectively. The matrix size was 128×92 pixels and the bandwidth 735 Hz/pixel. TE was fixed to 14 ms for the T1 measurements, and TR was fixed to 2,500 ms for the T2 measurements with variable TE. In both cases, two averages were acquired for each TI or TE.

#### Post-processing

The data were post-processed offline on a personal computer using in-house-built software PMI 0.4 [32].

Parameters were determined in patients with benign and malignant lesions. In the case of T1 and T2, values of water and fat were measured separately. The diffusivity of the fat component is negligible ( $ADC_{fat} < 0.1 \times 10^{-3}$  mm<sup>2</sup>/s) [13] and was not measured.

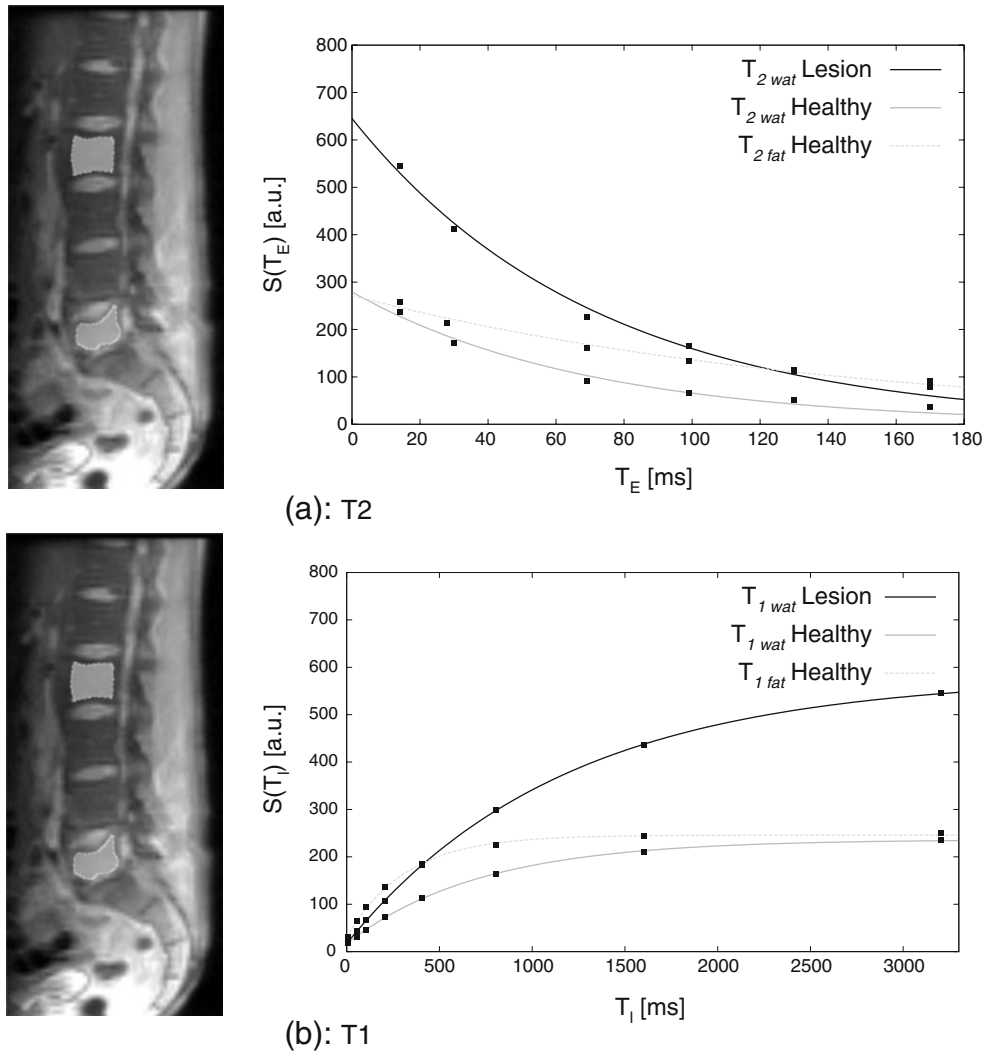


**Fig. 3** Reference images and the corresponding fits to the signal models for the ROI data. (a) Fit to the monoexponential decay model as a function of TE, the reference image corresponds to the

fat-saturated image with TE=14 ms; (b) fit to saturation recovery model, reference image corresponds to the fat-saturated image with TI=3,200 ms

Vertebrae were classified as appearing normal or abnormal according to their appearance on T1-weighted and STIR images by the consensus decision of two experienced radiologists (A.B., G.S.). An acute fracture was defined as a hyperintense region on the STIR images. Old fractures (without any signs of vBM oedema, i.e. the absence of a hyperintense region on the STIR image) or diffusely infiltrated vertebrae (manifested as a homogeneous signal reduction on unenhanced T1-weighted images) were excluded.

ROIs for T1 quantification were selected manually in the lesions on the fat-saturated image with the longest saturation time and in the normal-appearing vertebrae on the water-saturated image with the longest saturation time, providing the best contrast between vertebral bodies and intervertebral discs. T1 was calculated fitting signal intensities of the ROIs for varying TIs to a monoexponential saturation-recovery model [33]. The ROIs from the T1 quantification were used for T2 quantification and

corrected manually if necessary. T2 was quantified, fitting signal intensities for varying TEs to a monoexponential decay model [34].

For ADC quantification, the same ROIs were used and corrected manually according to their appearance on the image with the lowest diffusion weighting. Signal intensities for varying b-values were fitted to a monoexponential decay model using a least-squares algorithm to determine ADCs [35].

In addition, parameter maps were calculated by determining the value of each parameter on a voxel basis.

#### Statistical evaluation

Mean values and standard deviations of the parameters for both types of lesions and for normal-appearing vBM were determined. To compare normal-appearing vBM and lesions within one patient group, a paired two-tailed t-test

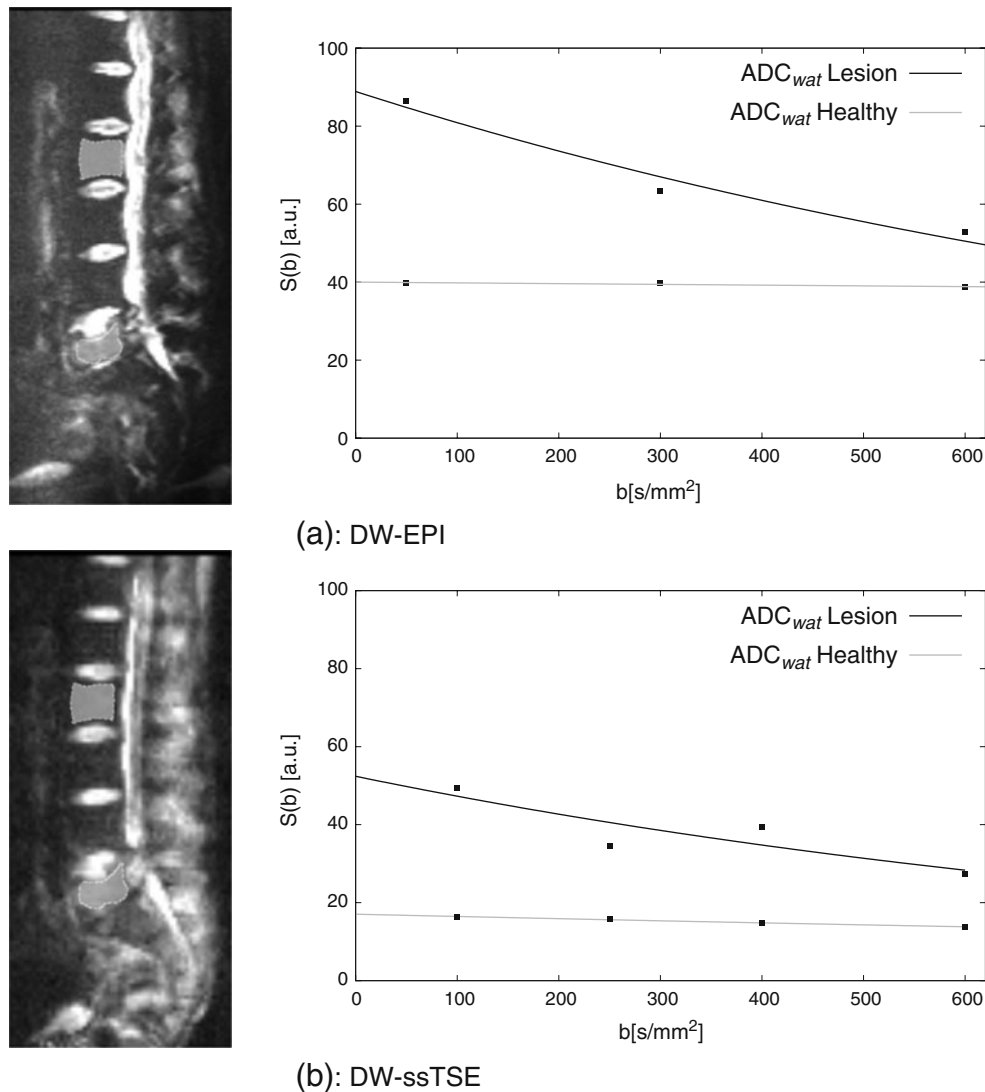


**Fig. 4** Fits to the monoexponential decay model as a function of the b-value for (c) DW-EPI; the reference image corresponds to  $b=50$  s/mm<sup>2</sup> and (d) DW-ssTSE; the reference image corresponds to  $b=100$  s/mm<sup>2</sup>

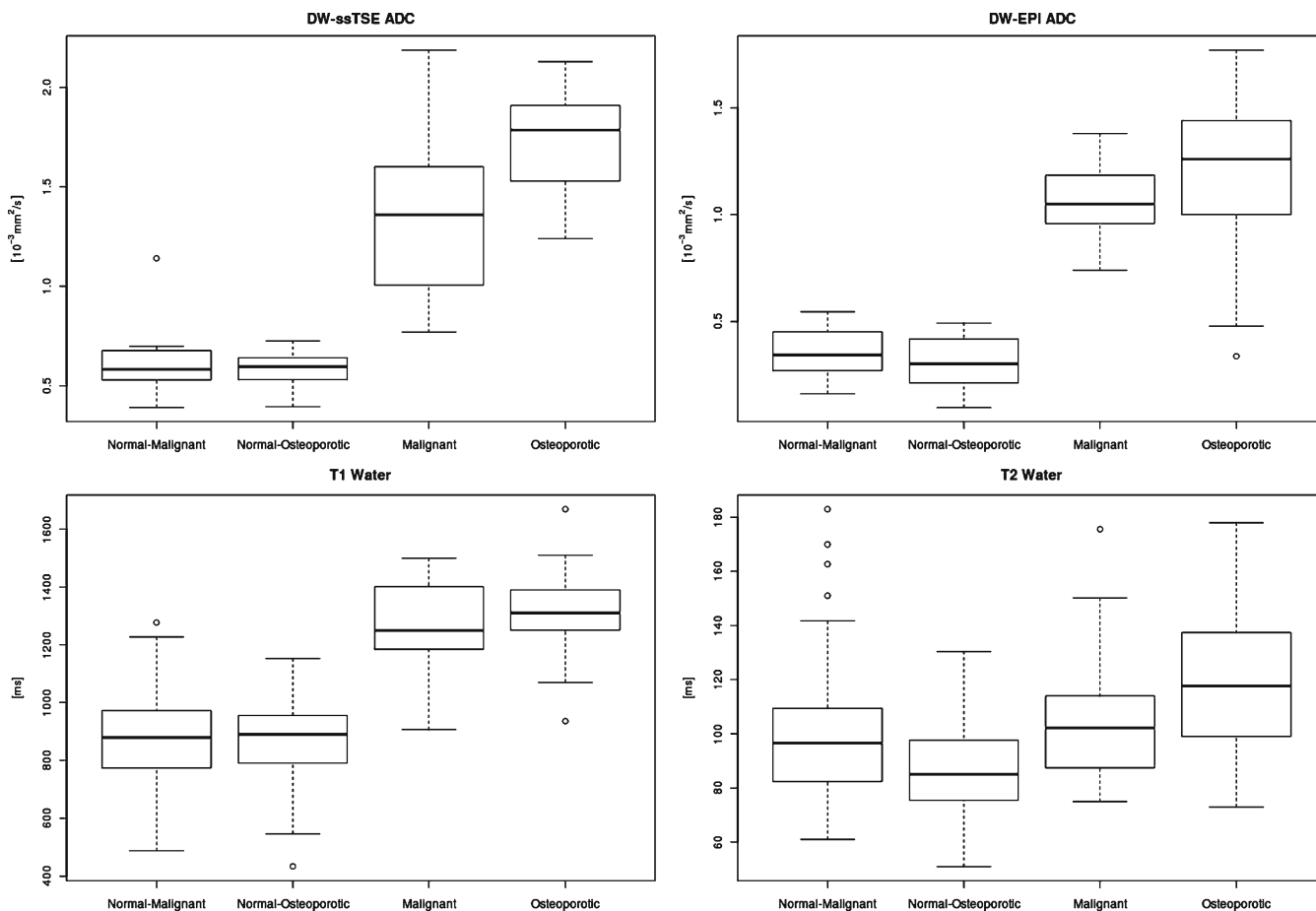


**Fig. 5** Boxplots summarising the values of the ADCs determined with the DW-ssTSE (upper left) and the DW-EPI (upper right) and the T1- (lower left) and the T2 values (lower right) of the water

component. Shown are the values in normal-appearing vBM and in the lesions of patients with osteoporosis and patients with malignant lesions

was performed. To compare parameters in normal-appearing vBM and lesions between both patient groups, an unpaired two-tailed t-test was performed.

In each patient, the inpatient variability (IPV) of each parameter was calculated. It was defined as the standard deviation of a parameter over all normal-appearing vertebrae per patient (evaluating one ROI for each vertebra). The values were normalised to the mean value in normal-appearing vBM of the corresponding patient. The ratio between the mean value in normal-appearing vBM and the lesion was calculated.

Correlations among T1, T2 and ADC measurements were assessed using Pearson’s product-moment correlation coefficient, and its significance was determined using a one-tailed paired t-test.

Accuracies, specificities and sensitivities of the parameters for the detection of malignant lesions [to be differentiated from osteoporotic (benign) lesions] were calculated. As a cutoff value, the parameter yielding the highest accuracy was chosen. To analyse whether a combined classification based on two parameters increases the accuracy, Fisher’s linear discriminant analysis was performed.

**Table 1** Summary of T1, T2 and ADC values in normal-appearing vBM and in lesions of patients with malignant infiltrations or benign osteoporotic fractures. The mean values are shown together with the standard deviations in parentheses

Tissue	Parameter	T1 [ms]		T2 [ms]		ADC [ $10^{-3} \text{ mm}^2/\text{s}$ ]	
		Water	Fat	Water	Fat	DW-ssTSE	DW-EPI
Normal-appearing vBM							
	Osteoporotic ( $n=147$ )	872 (129)	324 (81)	88 (16)	163 (32)	0.58 (0.17)	0.31 (0.15)
	Malignant ( $n=68$ )	878 (177)	386 (144)	99 (26)	146 (30)	0.62 (0.22)	0.35 (0.17)
Pathological condition							
	Osteoporotic ( $n=24$ )	1,315 (163)	–	122 (25)	–	1.74 (0.25)	1.17 (0.37)
	Malignant ( $n=20$ )	1,252 (157)	–	107 (26)	–	1.35 (0.41)	1.06 (0.19)

**Table 2** Summary of p-values of paired and unpaired t-tests for comparisons of ADCs as well as T1 and T2 relaxation times in water. For comparison between normal-appearing vBM and fracture-t-tests

Parameter	ADC(DW-ssTSE)	ADC(DW-EPI)	T1 water	T2 water
Normal-appearing vBM vs. lesion				
Osteoporotic ( <i>n</i> =20)	<b>&lt;0.0001</b>	<b>&lt;0.0001</b>	<b>&lt;0.0001</b>	<b>&lt;0.0001</b>
Malignant ( <i>n</i> =24)	<b>&lt;0.0001</b>	<b>&lt;0.0001</b>	<b>&lt;0.0001</b>	0.17
Osteoporotic vs. malignant				
Normal vBM ( <i>n</i> =147 vs. 68)	0.63	0.33	0.91	0.15
Lesion ( <i>n</i> =24 vs. 20)	<b>0.0008</b>	0.21	0.20	0.055

tures, a paired t-test and in the case of osteoporotic vs. malignant parameters an unpaired t-test was performed. Significant differences ( $p < 0.05$ ) are denoted by bold figures

## Results

Parameter maps for each parameter were calculated, and exemplary images are shown in Figs. 1 and 2. For the subsequent statistical analysis, the parameters were determined on a ROI basis. In total, 12 pathological fractures, 8 malignant infiltrations (tumour or metastasis) and 24 osteoporotic fractures were evaluated. Additionally, 68 ROIs in normal-appearing vBM in patients with malignant lesions and 147 ROIs in patients with benign lesions were evaluated. In six patients with a malignant lesion, all vertebrae showed signs of diffuse infiltration and hence a determination of values in normal-appearing vBM was not possible. T1 and T2 relaxation times of the fat component could not be determined in the lesions, as the water-saturated signal was too low because of a negligible fat fraction. In two patients with malignant lesions, the T2 values of water could not be evaluated because of poor image quality. In one patient with a malignant lesion, the DW-EPI sequence could not be evaluated because of poor image quality. Exemplary fits of the ROI data to the different models for ADC, T1 and T2 quantification are shown in Figs. 3 and 4.

The results for the different parameters are summarised in the boxplots in Fig. 5. The values in normal-appearing vBM and in the lesions of patients with osteoporotic or malignant lesions are shown separately. The mean values and standard deviations corresponding to these plots are summarised in Table 1. In addition, the values of the relaxation times of the fat component in normal-appearing vBM are shown.

Except for the T1 and T2 values of the fat component, which could not be determined in the fractures, the p-values of the comparisons of each parameter between the different subgroups are summarised in Table 2. Significant differences between normal-appearing vBM and the

lesions were found in both patient groups for each of the measured parameters ( $p < 0.01$ ), except for T2 of water in patients with malignant lesions ( $p = 0.17$ ). Comparing normal-appearing vBM of both patient groups, no significant differences for any of the parameters were found. In the case of the lesions, only the ADCs determined with the DW-ssTSE differed significantly ( $p < 0.001$ ). The T2 of water exhibited almost significant differences between benign and malignant fractures ( $p = 0.055$ ).

In addition to the analysis of the parameters for the whole patient collective, the intra-patient variabilities of each parameter were calculated and are summarised in Table 3. The smallest IPVs (of about 10%) were found for the T1 and T2 relaxation times in water and for the T2 relaxation times in fat. The highest IPV was found for the ADCs determined with the DW-EPI sequence in normal-appearing vBM of patients with malignant lesions (35.1%).

Furthermore, the parameter ratio between normal-appearing vBM and the lesion was calculated for each patient and parameter. The mean values and standard deviations of these ratios are also summarised in Table 3. The ratios differed significantly from 1 ( $p < 0.001$ ) except for the T2 relaxation time in patients with malignant lesions ( $p = 0.077$ ). The highest separation was found for the ADCs measured with the DW-EPI (malignant: 3.57 and osteoporotic: 4.25) and the DW-ssTSE (malignant: 2.43 and osteoporotic: 3.03).

Possible correlations among the different parameters were evaluated, and the results of the Pearson's product-moment correlation coefficient among the different parameters in the different subgroups are summarised in Table 4. Significant correlations ( $p < 0.05$ ) were found between the ADCs determined with the DW-ssTSE and DW-EPI sequence in normal-appearing vBM of patients with osteoporosis and in malignant lesions, between T1 and T2 of water in osteopor-

**Table 3** Mean values of the intra-patient variabilities (IPV) of the parameters in normal-appearing bone marrow and of the ratios between the values in the lesion and normal-appearing vBM (lesion/normal). The variabilities are given as the percentage of the

Parameter	ADC(DW-ssTSE)	ADC(DW-EPI)	T1 water	T2 water	T1 fat	T2 fat
IPV [%]						
Malignant	15.2 (8.4)	35.1 (23.2)	10.5 (9.3)	11.3 (8.6)	24.8 (20.3)	11.4 (0.6)
Osteoporotic	21.0 (13.6)	29.7 (16.0)	11.0 (4.5)	9.6 (5.1)	16.5 (10.2)	9.7 (4.0)
Lesion/normal						
Malignant	<b>2.43 (0.67)</b>	<b>3.57 (1.44)</b>	<b>1.43 (0.19)</b>	1.16 (0.32)	–	–
Osteoporotic	<b>3.03 (0.62)</b>	<b>4.25 (1.61)</b>	<b>1.52 (0.23)</b>	<b>1.39 (0.23)</b>	–	–

mean value (standard deviations in parentheses). For the ratios, a significant difference ( $p < 0.05$ ) from the hypothesis lesion/normal = 1 is denoted by bold figures

**Table 4** Summary of Pearson's product-moment correlation coefficients among the different parameters for the different subgroups. Significant correlations ( $p < 0.05$ ) are denoted by bold figures

Pearson's product-moment correlation coefficient	Normal-appearing vBM		Lesion	
	Osteoporosis	Malignant	Osteoporosis	Malignant
ADC(DW-ssTSE) vs. ADC(DW-EPI)	<b>0.66</b>	0.43	0.26	<b>0.76</b>
T1 vs. T2	0.18	0.01	<b>0.49</b>	<b>0.52</b>
T1 vs. ADC(DW-ssTSE)	<b>0.51</b>	<b>0.79</b>	0.20	0.31
T2 vs. ADC(DW-ssTSE)	0.25	0.19	-0.11	0.34
T1 vs. ADC(DW-EPI)	<b>0.73</b>	0.35	<b>0.53</b>	0.28
T2 vs. ADC(DW-EPI)	0.30	0.20	0.41	0.36

otic and malignant lesions, between T1 of water and DW-ssTSE ADCs in osteoporotic and malignant normal-appearing vBM, and between T1 of water and DW-EPI ADCs in osteoporotic normal-appearing vBM and osteoporotic fractures.

Finally, the specificities and sensitivities of the different parameters for the differentiation between osteoporotic and malignant lesions were analysed; the results are summarised in Table 5. The highest accuracy of 77% was found for the ADC determined with the DW-ssTSE sequence. For a cutoff value of  $1.49 \times 10^{-3} \text{ mm}^2/\text{s}$ , a sensitivity of 65% and a specificity of 88% were found. For the other parameters, the accuracies were found to be smaller. Fisher's linear discriminant analysis showed that for a combined classification based on T2 and DW-ssTSE ADCs, the accuracy could be increased to 88%, corresponding to a sensitivity of 78% and a specificity of 96%. The linear discriminant corresponds to a rotation of the x-axis (corresponding to the ADC) by  $31^\circ$  as shown in Fig. 6. All other combinations of measured parameters did not increase the accuracy compared with the evaluation of the DW-ssTSE ADC alone.

## Discussion

Historically, relaxation times as well as apparent diffusion coefficients of vBM were determined as bulk values, representing a mixture of fat and water. Since the values in fat and water show substantial differences when determining bulk values in different patients and pathological conditions, differences might not only be related to a change in the physical parameter but also to a change in the tissue composition. A separate determination of relaxation times and ADCs for both components might avoid this misinterpretation.

**Table 5** Sensitivities, specificities, accuracies, positive predictive values (PPV) and negative predictive values (NPV) of the different parameters with respect to the diagnosis of a malignant lesion

Parameter	Cutoff	Sensitivity	Specificity	Accuracy
ADC(DW-ssTSE) [ $10^{-3} \text{ mm}^2/\text{s}$ ]	1.49	0.65 (13/20)	0.88 (21/24)	0.77
ADC(DW-EPI) [ $10^{-3} \text{ mm}^2/\text{s}$ ]	1.12	0.68 (13/19)	0.65 (15/23)	0.67
T1-water [ms]	1262	0.60 (12/20)	0.75 (18/24)	0.68
T2-water [ms]	114	0.78 (14/18)	0.67 (16/24)	0.71
ADC(DW-ssTSE) and T2-water	1.29/119 <sup>a</sup>	0.78 (14/18)	0.96 (23/24)	0.88

<sup>a</sup> Cutoff in the combined case corresponds to a point on the linear discriminant. All points fulfilling the condition:  $-\tan(31^\circ) (T2 - \text{water} - 119\text{ms}) / (103\text{ms}) + (\text{ADC} - 1.29 \times 10^{-3} \text{ mm}^2/\text{s}) / (1.34 \times 10^{-3} \text{ mm}^2/\text{s}) < 0$  are classified as malignant. 103 ms and  $1.34 \times 10^{-3} \text{ mm}^2/\text{s}$  correspond to the difference between maximum and minimum of T2 and ADC values in the lesions and were used for normalisation of the data;  $31^\circ$  is the angle between the linear discriminant and the ADC axis

## T1 relaxation

T1 of water and fat protons has only been measured in a few studies. Our values for T1 of the water component in normal-appearing vBM of 872 ms in patients with osteoporosis and of 878 ms in patients with malignant infiltration agree with the measurements of Träber et al. at 1.5 T [14]. The T1 values of the fat component (386 and 324 ms) are somewhat higher than those of 260–290 ms obtained in [14, 15]. The standard deviations and the IPV of T1 in fat are relatively large, possibly caused by partially insufficient water suppression in the present study. Träber et al. performed a spectroscopic measurement, which does not suffer from any imperfect suppression effects. Gold et al. [15] used a spectral-spatial excitation pulse.

It was shown by Sugimura et al. [23] at 0.15 T that bulk T1 of malignant metastatic lesions was longer than that of non-neoplastic ones. Träber et al. at 1.5 T reported an increase in T1 of water of 16% in malignant lesions compared with normal vBM [14]. We found an increase of 43% in malignant lesions compared with normal-appearing vBM in the same patient, possibly explained by the higher ratio of free to fixed water in tumours. Ito et al. [36] found a positive correlation between the BMD and T1 of water at 1.5 T. Conversely, Träber et al. found no significant differences between normal-appearing vBM of patients with and without osteoporosis. This agrees with our results, showing no significant differences between T1 in normal-appearing vBM of patients with osteoporosis and those with malignant lesions. Here, for the first time, the T1 of water in osteoporotic fractures was determined. It was found to be increased by 52%; possibly, the free water in the bone marrow oedema is responsible for this increase.



## T2 relaxation

T2 of water in vBM has previously been measured only by Träber et al. Our values of 88 ms in normal-appearing vBM of patients with osteoporosis and 99 ms in patients with malignant lesions are about 30% higher. T2 of fat in vBM was determined by Gold et al. as 166 ms, agreeing well with our values in normal-appearing vBM of 163 ms in patients with osteoporosis and 146 ms in patients with malignant lesions. The values reported by Träber et al. of about 70 ms

are 50% smaller than our results. Interestingly, the T2 values of fat measured by Gold et al. agree, while the T1 values of fat disagree with our results although the same technique of fat suppression was applied in both cases [15].

In malignant lesions, an increase of 16% of T2 was found compared with normal-appearing vBM. These differences were not significant, contrary to the findings of Träber et al. reporting a significant difference ( $p < 0.002$ ). T2 in osteoporotic fractures has not been determined before. A significant increase of 39% was found, possibly caused by a reduction

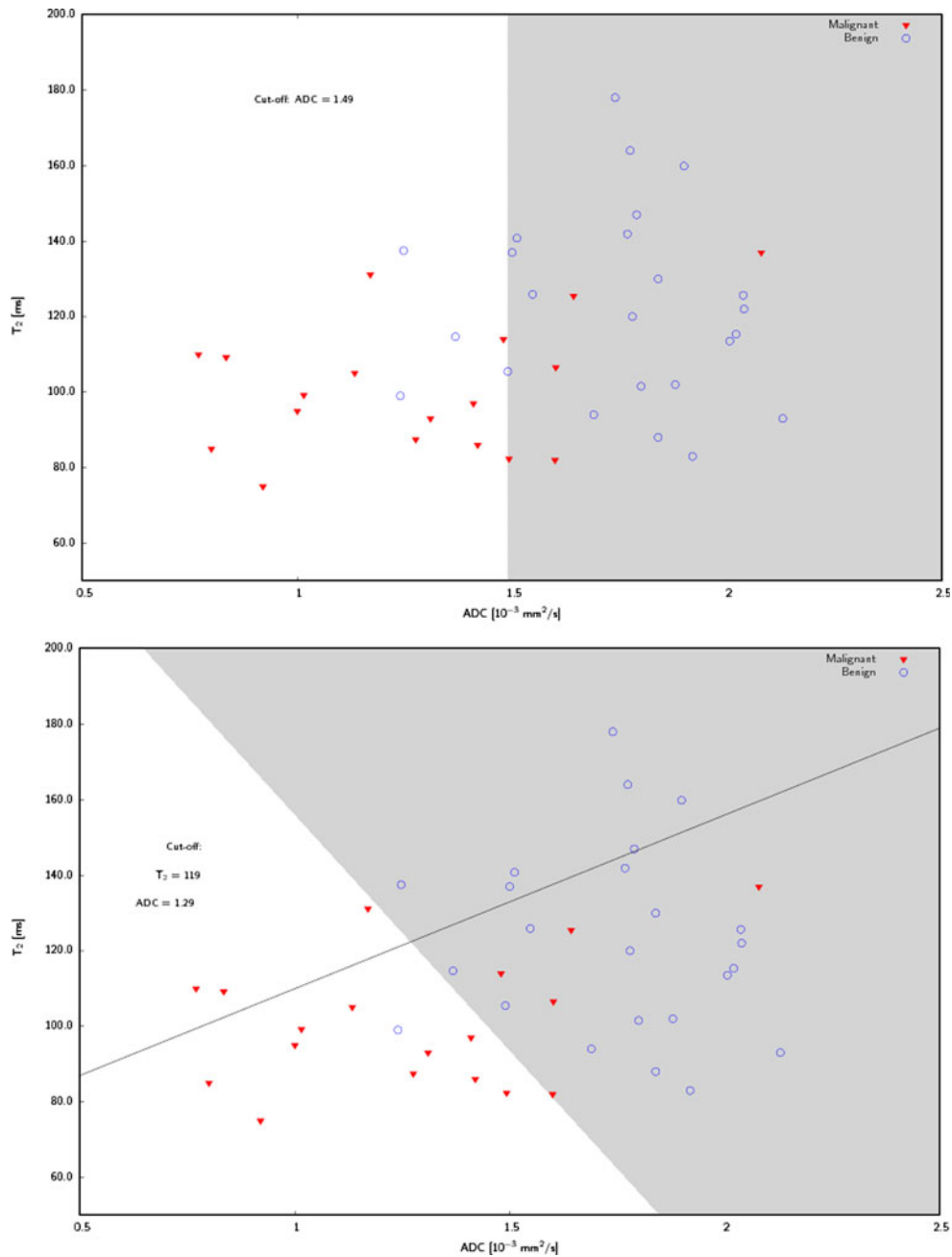


**Fig. 6** Scatterplots of the ADC(ssTSE) vs. T2. In the upper figure, the separation between malignant and benign lesions based on the ADC is shown. The white area corresponds to a classification as malignant fractures. In the lower plot, the linear discriminant for a

classification based on T2 and ADC is shown as the black line. The cutoff separating the grey and white areas corresponds to the intersection of the grey border with the linear discriminant

of local magnetic field gradients caused by the destruction of the trabecular structure.

#### Apparent diffusion coefficients

Typical ADCs in the literature vary from 0.2 to  $0.5 \times 10^{-3} \text{ mm}^2/\text{s}$  [37]. The general variability can be explained by the different pulse sequences and diffusion weightings used. The most important difference is the application of fat saturation; typical values with fat saturation are in the range of 0.3 to  $0.5 \times 10^{-3} \text{ mm}^2/\text{s}$ . Our ADCs obtained with the DW-ssTSE and DW-EPI differ significantly. The SNR of the DW-ssTSE sequence at higher b-values was higher than that of the DW-EPI sequence. Thus, the signal attenuation of the DW-EPI sequence is underestimated yielding lower estimates for the ADCs. Furthermore, the DW-EPI images suffered from gross geometrical image distortions caused by susceptibility heterogeneities. Because of these limitations, the DW-ssTSE appears to be the preferable sequence in the vertebral column.

In the lesions, the ADCs are substantially increased compared with normal-appearing vBM. The effect of the underestimation of ADCs is more important in normal-appearing vBM; thus, the ratios between the lesion and normal-appearing vBM are higher for the DW-EPI sequence.

#### Lesion differentiation

We investigated the potential of the various parameters determined in this study for the differentiation. The only parameter that provided a significant difference was the ADC, which is in agreement with previous studies [25–27, 30, 31, 38, 39]. However, an overlap between the two groups exists and therefore the sensitivity (65%) and the specificity (88%) are not high enough to replace the usual diagnosis based on the histological validation. An improvement of the diagnostic accuracy compared with each of the evaluated parameters alone was possible when ADC and T2 were

combined. Using the linear discriminant based on T2 and ADC, we obtained a sensitivity of 78% and a specificity of 96%. This value is lower than the values reported based on the differentiation based on qualitative criteria [16–22], which might partially be explained by the relatively low number of patients included in the present study. However, quantitative parameters might provide additional information, especially in the cases where the cause of the fracture is not apparent on conventional MR imaging. The combination of qualitative and quantitative criteria might provide the best differentiation in these cases.

Non-quantitative diffusion-weighted imaging has also been successfully applied for lesion differentiation using diffusion-weighted steady-state free-precession (DW-SSFP) sequences [40–45]. The signal of the DW-SSFP sequence is a very complex function of the ADCs and the relaxation times [46]. The exact contrast mechanism resulting in the excellent lesion differentiation is not yet fully understood. The parameters quantified in the present study might be important input parameters for a better understanding of the different signal behaviour of the DW-SSFP sequence.

#### Conclusion

For the first time, vertebral T1 and T2 relaxation times of the fat and water components, and ADCs were measured in patients presenting with vertebral lesions. All parameters exhibit significant differences between normal-appearing vBM and the lesions. However, only the ADCs determined with a DW-ssTSE technique showed significant differences between osteoporotic fractures and malignant lesions and might be helpful for the differential diagnosis of these two entities.

**Acknowledgements** This work was supported by the Deutsche Forschungsgemeinschaft (DFG), grant no. DI 1413/1-1.

#### References

- Vogler JB, Murphy WA (1988) Bone marrow imaging. *Radiology* 168:679–693
- Wehrli FW, MacFall JR, Shotts D et al (1984) Mechanisms of contrast in NMR imaging. *J Comput Assist Tomogr* 8:369–380
- Vande Berg CV, Malghem J, Lecouvet FE et al (1998) Magnetic resonance imaging of the normal bone marrow. *Skeletal Radiol* 27:471–483
- Bottomley PA, Foster TH, Argesersinger RE et al (1984) A review of normal tissue hydrogen NMR relaxation times and relaxation mechanisms from 1–100MHz: dependence on tissue type, NMR frequency, temperature, species, excision, and age. *Med Phys* 11:425–448
- Dooms GC, Fisher MR, Hricak H et al (1985) Bone marrow imaging: magnetic resonance studies related to age and sex. *Radiology* 155:429–432
- Richards MA, Webb JA, Jewell SE (1988) In-vivo measurement of spin lattice relaxation time (T1) of bone marrow in healthy volunteers: the effects of age and sex. *Br J Radiol* 61:30–33
- De Bazelaire CMJ, Duhamel G, Rofsky NM et al (2004) MR imaging relaxation times of abdominal and pelvic tissues measured in vivo at 3.0T: preliminary results. *Radiology* 230:652–659
- Dietrich O, Herlihy A, Dannels WR et al (2001) Diffusion-weighted imaging of the spine using radial k-space trajectories. *MAGMA MagnReson Mater Phy* 12:23–31
- Byun WM, Shin SO, Chang Y et al (2002) Diffusion-weighted MR imaging of metastatic disease of the spine: assessment of response to therapy. *AJNR Am J Neuroradiol* 23:906–912
- Bammer R, Herneth AM, Maier SE et al (2003) Line scan diffusion imaging of the spine. *AJNR Am J Neuroradiol* 24:5–12

11. Yeung DKW, Wong SYS, Griffith JF et al (2004) Bone marrow diffusion in osteoporosis: evaluation with quantitative MR diffusion imaging. *J Magn Reson Imaging* 19:222–228
12. Griffith JF, Yeung DKW, Antonio GE et al (2006) Vertebral marrow fat content and diffusion and perfusion indexes in women with varying bone density: MR evaluation. *Radiology* 241:831–838
13. Ward R, Caruthers S, Yablon C et al (2000) Analysis of diffusion changes in posttraumatic bone marrow using navigator-corrected diffusion gradients. *AJR Am J Roentgenol* 174:731–734
14. Träber F, Block W, Layer G et al (1996) Determination of 1H relaxation times of water in human bone marrow by fat-suppressed turbo spin echo in comparison to MR spectroscopic methods. *J Magn Reson Imaging* 6:541–548
15. Gold GE, Han E, Stainsby J et al (2004) Musculoskeletal MRI at 3.0 T: relaxation times and image contrast. *AJR Am J Roentgenol* 183:343–351
16. Frager D, Elkin C, Swerdlow M (1988) Subacute osteoporotic compression fracture: misleading magnetic resonance appearance. *Skeletal Radiol* 17:123–126
17. Yuh WT, Zachar CK, Barloon TJ et al (1989) Vertebral compression fractures: distinction between benign and malignant causes with MR imaging. *Radiology* 172:215–218
18. Baker LL, Goodman SB, Perkash I (1990) Benign versus pathologic compression fractures of vertebral bodies: assessment with conventional spin-echo, chemical-shift, and STIR MR imaging. *Radiology* 174:495–502
19. Rupp RE, Ebraheim NA, Coombs RJ (1995) Magnetic resonance imaging differentiation of compression spine fractures or vertebral lesions caused by osteoporosis or tumor. *Spine* 20:499–503
20. Cuenod CA, Laredo JD, Chevret S et al (1996) Acute vertebral collapse due to osteoporosis or malignancy: appearance on unenhanced and gadolinium-enhanced MR images. *Radiology* 199:541–549
21. Shih TT, Huang KM, Li YW (1999) Solitary vertebral collapse: distinction between benign and malignant causes using MR patterns. *J Magn Reson Imaging* 9:635–642
22. Jung H, Jee W, McCauley TR et al (2003) Discrimination of metastatic from acute osteoporotic compression spinal fractures with MR imaging. *Radiographics* 23:179–187
23. Sugimura K, Yamasaki K, Kitagaki H et al (1987) Bone marrow diseases of the spine: differentiation with T1 and T2 relaxation times in MR imaging. *Radiology* 165:541–544
24. Sundaram M, McGuire MH, Schajowicz F (1987) Soft-tissue masses: histologic basis for decreased signal (short T2) on T2-weighted MR images. *AJR Am J Roentgenol* 148:1247–1250
25. Herneth AM, Naude J, Philipp M et al (2000) The value of diffusion-weighted MRT in assessing the bone marrow changes in vertebral metastases. *Radiologie* 40:731–736
26. Chan JHM, Peh WCG, Tsui EYK et al (2002) Acute vertebral body compression fractures: discrimination between benign and malignant causes using apparent diffusion coefficients. *Br J Radiol* 75:207–214
27. Zhou XJ, Leeds NE, McKinnon GC et al (2002) Characterization of benign and metastatic vertebral compression fractures with quantitative diffusion MR imaging. *AJNR Am J Neuroradiol* 23:165–170
28. Maeda M, Sakuma H, Maier SE et al (2003) Quantitative assessment of diffusion abnormalities in benign and malignant vertebral compression fractures by line scan diffusion-weighted imaging. *AJR Am J Roentgenol* 181:1203–1209
29. Oner AY, Tali T, Celikyay F et al (2007) Diffusion-weighted imaging of the spine with a non-Carr-Purcell-Meiboom-Gill single-shot fast spin-echo sequence: initial experience. *AJNR Am J Neuroradiol* 28:575–580
30. Raya JG, Dietrich O, Birkenmaier C et al (2007) Feasibility of a RARE-based sequence for quantitative diffusion-weighted MRI of the spine. *Eur Radiol* 17:2872–2879
31. Balliu E, Vilanova JC, Peláez I et al (2009) Diagnostic value of apparent diffusion coefficients to differentiate benign from malignant vertebral bone marrow lesions. *Eur J Radiol* 69:560–566
32. Sourbron S, Biffar A, Ingrisich M et al (2009) PMI: Platform for Research in Medical Imaging. *ESMRMB09 Antalya, 2009 MAGMA Magn Reson Mater Phys*. 22 (Suppl. 1):539
33. Crawley AP, Henkelman RM (1988) A comparison of one-shot and recovery methods in T1 imaging. *Magn Reson Med* 7:23–34
34. Abragam A (2004) Principles of nuclear magnetism. Oxford University Press, New York
35. Stejskal EO, Tanner JE (1965) Spin Diffusion Measurements: Spin Echoes in the Presence of a Time-Dependent Field Gradient. *J Chem Phys* 42:288–292
36. Ito M, Hayashi K, Uetani M et al (1993) Bone mineral and other bone components in vertebrae evaluated by QCT and MRI. *Skeletal Radiol* 22:109–113
37. Dietrich O, Biffar A, Reiser M et al (2009) Diffusion-weighted imaging of bone marrow. *Semin Musculoskelet Radiol* 13:134–144
38. Herneth A, Philipp M, Naude J et al (2002) Vertebral metastases: assessment with apparent diffusion coefficient. *Radiology* 225:889–894
39. Tang G, Liu Y, Li W et al (2007) Optimization of b value in diffusion-weighted MRI for the differential diagnosis of benign and malignant vertebral fractures. *Skeletal Radiol* 36:1035–1041
40. Baur A, Stähler A, Brünig R et al (1998) Diffusion-weighted MR imaging of bone marrow: differentiation of benign versus pathologic compression fractures. *Radiology* 207:349–356
41. Abanoz R, Hakyemez B, Parlak M (2003) Diffusion-weighted imaging of acute vertebral compression: Differential diagnosis of benign versus malignant pathologic fractures. *Tani Girisim Radyol* 9:176–183
42. Hackländer T, Scharwächter C, Golz R et al (2006) Value of diffusion-weighted imaging for diagnosing vertebral metastases due to prostate cancer in comparison to other primary tumors. *Rofo* 178:416–424
43. Byun WM, Jang HW, Kim SW et al (2007) Diffusion-weighted magnetic resonance imaging of sacral insufficiency fractures: comparison with metastases of the sacrum. *Spine* 32:820–824
44. Castillo M, Arbelaez A, Smith JK et al (2000) Diffusion-weighted MR imaging offers no advantage over routine noncontrast MR imaging in the detection of vertebral metastases. *AJNR Am J Neuroradiol* 21:948–953
45. Baur A, Huber A, Dürr HR et al (2002) Differentiation of benign osteoporotic and neoplastic vertebral compression fractures with a diffusion-weighted, steady-state free precession sequence. *Rofo* 174:70–75
46. Buxton RB (1993) The diffusion sensitivity of fast steady-state free precession imaging. *Magn Reson Med* 29:235–243